

Predict to Skip: Linear Multistep Feature Forecasting for Efficient Diffusion Transformers

Hanshui Cui^{1,2} Zhiqing Tang¹ Qianli Ma² Zhi Yao^{1,2} Weijia Jia¹

Abstract

Diffusion Transformers (DiT) have emerged as a widely adopted backbone for high-fidelity image and video generation, yet their iterative denoising process incurs high computational costs. Existing training-free acceleration methods rely on feature caching and reuse under the assumption of temporal stability. However, reusing features for multiple steps may lead to latent drift and visual degradation. We observe that model outputs evolve smoothly along much of the diffusion trajectory, enabling principled predictions rather than naive reuse. Based on this insight, we propose **PrediT**, a training-free acceleration framework that formulates feature prediction as a linear multistep problem. We employ classical linear multistep methods to forecast future model outputs from historical information, combined with a corrector that activates in high-dynamics regions to prevent error accumulation. A dynamic step modulation mechanism adaptively adjusts the prediction horizon by monitoring the feature change rate. Together, these components enable substantial acceleration while preserving generation fidelity. Extensive experiments validate that our method achieves up to $5.54\times$ latency reduction across various DiT-based image and video generation models, while incurring negligible quality degradation.

1. Introduction

Generative AI has achieved remarkable success across a wide range of applications, such as image and video generation, and controllable content creation (Fui-Hoon Nah et al., 2023; Cao et al., 2025). Diffusion models (DMs) (Dhariwal & Nichol, 2021; Ho et al., 2020; Rombach et al., 2022)

¹School of Artificial Intelligence, Beijing Normal University, Beijing 100875, China ²Institute of Artificial Intelligence and Future Networks, Beijing Normal University, Zhuhai 519087, China. Correspondence to: Zhiqing Tang <zhiqing.tang@bnu.edu.cn>.

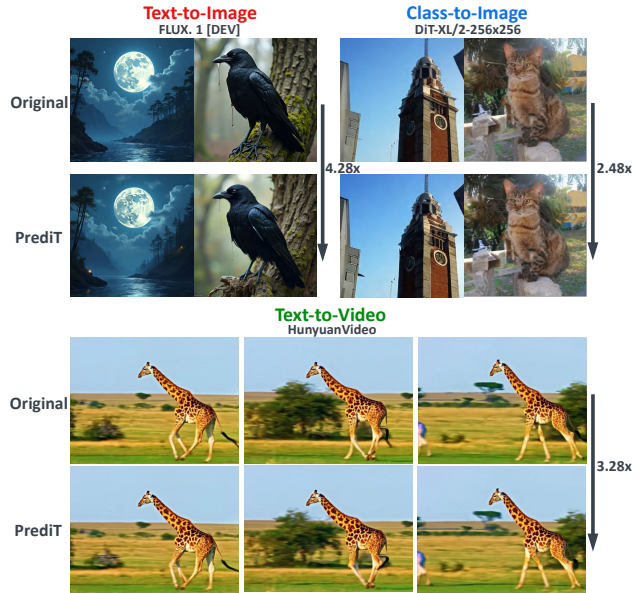


Figure 1. Accelerating Diffusion Transformer inference across multiple models. PrediT achieves significant speedup on various DiT-based architectures for both image and video generation while preserving visual quality.

generate data by learning to reverse a gradual noising process, becoming the foundation of these advances. Early DMs relied on U-Net (Blattmann et al., 2023; Ramesh et al., 2022) architectures, but the limited receptive field of convolutional networks makes it difficult to capture long-range dependencies, restricting generation quality for complex scenes. Diffusion Transformers (DiT) (Peebles & Xie, 2023) have been proposed to address this limitation, leveraging the self-attention mechanism to model global relationships across the entire latent space. DiT models are now a widely adopted backbone behind state-of-the-art models (Zheng et al., 2024; Chen et al., 2023b; 2024b; Liu et al., 2024; Esser et al., 2024). However, DiT inference is computationally expensive, as the quadratic attention cost combined with iterative denoising results in significant latency, making real-time generation impractical.

To accelerate DiT inference, two main categories of methods have been explored. Training-based approaches, such as distillation (Salimans & Ho, 2022; Meng et al., 2023)

and quantization (Shang et al., 2023; Li et al., 2023), reduce model complexity but require substantial training data and compute, and may degrade generation quality due to distribution shift. Training-free methods are increasingly popular due to their plug-and-play nature. Among these, caching-based approaches exploit the temporal redundancy in diffusion sampling by caching intermediate features and reusing them across consecutive steps, thereby reducing the number of full model samplings (Liu et al., 2025c).

Despite their efficiency, existing caching methods face limitations. Reuse-based methods such as DeepCache (Ma et al., 2024b), FORA (Selvaraju et al., 2024), and Δ -DiT (Chen et al., 2024c) directly substitute previous model outputs for current ones, assuming that features remain unchanged across steps. However, this assumption breaks down in regions of high-dynamics along the denoising trajectory, leading to latent drift and potentially causing visual artifacts. To maintain acceptable quality, these methods must limit their acceleration ratio, resulting in modest speedups. More advanced approaches such as AB-Cache (Yu et al., 2025) and TaylorSeer (Liu et al., 2025d) extrapolate future features from historical information. While these methods improve upon naive reuse, they still suffer from error accumulation under fixed skip intervals, especially when the model output exhibits non-uniform dynamics.

A key observation motivating our approach is that the model’s feature trajectory along the diffusion process is locally smooth (see Figure 2a), which suggests that the temporal structure of the denoising process can be exploited beyond naive reuse. To enable high-quality generation with aggressive acceleration, we identify two key challenges that must be addressed: **(1) How to predict accurately and stably?** Naive reuse is a zero-order approximation, while existing forecasting methods rely on finite-difference estimation that is sensitive to noise and unstable in higher-order terms, causing error accumulation under large skip intervals. **(2) How to adapt the prediction horizon dynamically?** The dynamics varies significantly throughout the diffusion trajectory, with the initial and final phases exhibiting rapid changes while middle timesteps are smooth. A fixed skip schedule cannot account for this variation, leading to over-skipping (quality loss) or under-skipping (limited speedup).

In this paper, we propose **PrediT (Predictive DiT)**, a training-free framework that treats feature estimation as a linear multistep prediction problem. We employ the Adams-Bashforth predictor, which directly combines historical function values without explicit derivative estimation, to extrapolate future model outputs with improved numerical stability. An Adams-Moulton corrector is further applied in high-dynamics regions to refine predictions and prevent error accumulation. A dynamic step modulation mechanism monitors the relative change rate and adaptively adjusts

how many steps can be safely skipped. In contrast to prior methods that either passively reuse stale features or apply fixed-interval extrapolation without adaptive control, PrediT allows principled prediction with adaptive step modulation, achieving aggressive acceleration without quality degradation. As shown in Figure 1, PrediT achieves $4.28\times$ speedup on FLUX (Labs et al., 2025), $2.48\times$ on DiT-XL/2 (Peebles & Xie, 2023), and $3.28\times$ on HunyuanVideo (Kong et al., 2024) while maintaining comparable visual fidelity. In summary, our main contributions are:

- We analyze why naive feature reuse leads to latent drift and show that diffusion trajectories are locally smooth, motivating higher-order polynomial prediction.
- We propose PrediT, a training-free framework employing the Adams-Bashforth predictor with Adams-Moulton correction for stable feature forecasting. A dynamic step modulation mechanism monitors relative feature change rate and adaptively adjusts the prediction interval.
- Extensive experiments on several DiT-based models demonstrate that PrediT achieves up to $5.54\times$ speedup while maintaining comparable generation quality, outperforming existing caching methods.

2. Related Work

Diffusion Models. Diffusion models (DMs) (Dhariwal & Nichol, 2021; Ho et al., 2020; Rombach et al., 2022) have achieved remarkable success across diverse generative tasks. These models generate high-quality samples by progressively denoising data through an iterative refinement process (Croitoru et al., 2023; Yang et al., 2023). Early diffusion models predominantly relied on U-Net architectures but exhibited challenges in capturing long-range dependencies across spatial regions (Chen et al., 2023a; 2024a). To address these limitations, Diffusion Transformers (DiTs) (Peebles & Xie, 2023) replace the U-Net backbone with a transformer-based architecture (Blattmann et al., 2023; Ramesh et al., 2022). Despite their impressive generation quality and scalability advantages, DiTs suffer from higher inference latency compared to their predecessors. This computational burden has motivated extensive research into accelerating DiT inference.

Efficient Diffusion Models. Numerous approaches have been proposed to accelerate diffusion models. DDIM (Song et al., 2020a) introduces a non-Markovian formulation that allows deterministic sampling with significantly fewer steps. Model complexity reduction methods primarily focus on distillation (Salimans & Ho, 2022; Meng et al., 2023) and quantization (Shang et al., 2023; Li et al., 2023), which transfer knowledge to smaller models or reduce numerical precision respectively. However, these methods often in-

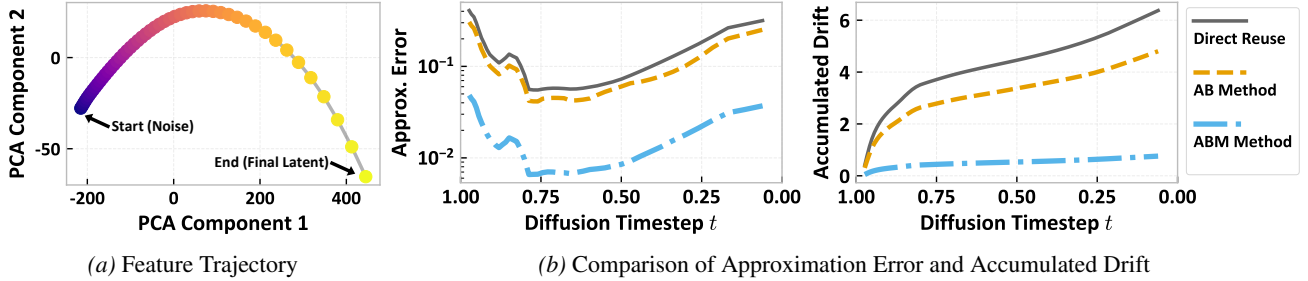


Figure 2. Analysis of direct feature reuse limitations. (a) Feature trajectory visualization via PCA shows local smoothness along the diffusion process. (b) Comparison of per-step approximation error and accumulated drift: naive reuse incurs significant error accumulation, while higher-order prediction methods reduce drift.

roduce notable trade-offs. Large sampling reduction can compromise generation quality and diversity, distillation requires substantial computational resources and may be limited by teacher model performance, and extreme quantization can lead to noticeable degradation in visual fidelity.

Diffusion Model Caching. Cache-based acceleration methods have emerged as a promising training-free paradigm that exploits temporal redundancy in the denoising process. DeepCache (Ma et al., 2024b) pioneers this approach by caching and reusing high-level features across adjacent denoising timesteps. Δ -DiT (Chen et al., 2024c) introduces a DiT-specific caching mechanism that stores feature differences rather than raw outputs. FORA (Selvaraju et al., 2024) implements a static caching strategy with a fixed interval parameter. More sophisticated approaches include PAB (Zhao et al., 2024), which applies different broadcast ranges for spatial, temporal, and cross-modal attention mechanisms. TeaCache (Liu et al., 2025a) intelligently determines when to use cached results based on input similarity. SmoothCache (Liu et al., 2025b) analyzes layer-wise representation errors from calibration data to adaptively determine caching intensity. ProfilingDiT (Ma et al., 2025a) distinguishes foreground-focused and background-focused transformer blocks, selectively caching static background features.

While these direct feature reuse methods show impressive acceleration, they rely on features from previous timesteps that may not perfectly align with the current denoising stage, causing accumulated errors that manifest as artifacts or quality loss. An alternative approach involves predicting future timestep features rather than directly reusing cached results. TaylorSeer (Liu et al., 2025d) employs Taylor series expansion to forecast features at future timesteps. AB-Cache (Yu et al., 2025) provides theoretical justification through the Adams-Bashforth numerical method, revealing a linear relationship between outputs of consecutive denoising steps. ABM-Solver (Ma et al., 2025b) extends this framework for inversion and editing tasks. Yet these prediction-based methods adopt fixed skip intervals without adaptive control, leading to error accumulation when feature dynamics vary

significantly across the diffusion trajectory.

3. Method

We present PrediT, a training-free acceleration framework for DiTs that formulates feature prediction as a linear multistep problem. We first analyze the limitations of existing reuse-based methods and the smoothness property of diffusion trajectories, then introduce our predictor-corrector scheme with dynamic step modulation.

3.1. Preliminaries

Diffusion Models. DMs generate data by learning to reverse a gradual noising process. Given clean data x_0 , a forward process progressively adds Gaussian noise over timesteps $t \in [0, 1]$ to produce x_t . The reverse process starts from pure noise $x_1 \sim \mathcal{N}(0, I)$ and iteratively denoises to recover x_0 . It can be formulated as solving an Ordinary Differential Equation (ODE) (Song et al., 2020a;b):

$$\frac{dx}{dt} = f_\theta(x_t, t), \quad (1)$$

where f_θ is the model’s velocity prediction (Lipman et al., 2022). The solution is obtained by numerical integration from $t = 1$ to $t = 0$.

Diffusion Transformers. Diffusion Transformers (DiT) (Peebles & Xie, 2023) replace the U-Net backbone with a transformer architecture. The latent z_t is patchified into tokens, processed through self-attention and MLP layers, and unpatchified back to latent dimensions. Each DiT block applies Adaptive Layer Normalization (AdaLN) conditioned on timestep t :

$$h' = \text{Attn}(\text{AdaLN}(h)), \quad h'' = \text{MLP}(\text{AdaLN}(h')). \quad (2)$$

While DiT achieves superior generation quality, the quadratic attention cost combined with dozens of iterative steps makes inference computationally expensive.

Feature Reuse. Current caching methods accelerate inference by reusing previous model outputs (Ma et al., 2024b;

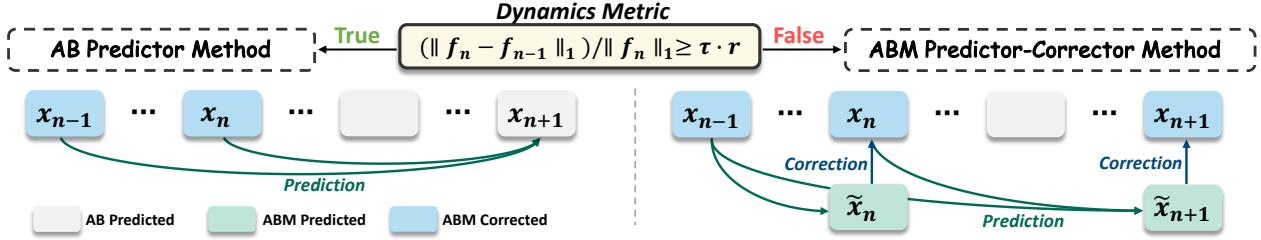


Figure 3. Overview of the PrediT framework. PrediT formulates feature prediction as a linear multistep problem, using historical model outputs to extrapolate future features and reduce redundant model calls. The threshold τ and correction ratio r control the selection between ABM for high-dynamics and AB for low-dynamics regions.

Chen et al., 2024c). Given the current state x_n at timestep t_n , these methods approximate the model output as:

$$\hat{f}_n \approx f_{n-k}, \quad (3)$$

where f_{n-k} is a cached output from k steps earlier. This zero-order approximation assumes f remains constant, incurring a local truncation error (LTE) of $\mathcal{O}(\Delta t)$. This error accumulates over consecutive skips, causing latent drift and visual artifacts.

Linear Multistep Methods. Linear multistep methods (Hairer et al., 1993; Butcher, 2016) are classical numerical techniques for solving ODEs that use multiple previous function values to achieve higher-order accuracy. Starting from the integral form of Equation (1):

$$x_{n+1} = x_n + \int_{t_n}^{t_{n+1}} f(x(s), s) ds, \quad (4)$$

these methods approximate the integrand by a polynomial interpolating past values $\{f_n, f_{n-1}, \dots\}$, achieving LTE of $\mathcal{O}(\Delta t^{k+1})$ for order k . This provides a principled framework for predicting model outputs without explicit derivative estimation (Lu et al., 2022; 2025).

3.2. PrediT Framework

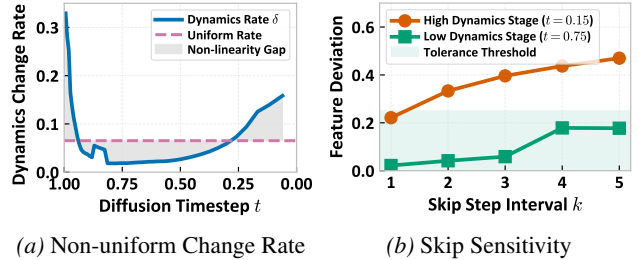
As illustrated in Figure 3, PrediT combines an Adams-Bashforth predictor with an Adams-Moulton corrector under dynamic step modulation.

Adams-Bashforth Predictor. The Adams-Bashforth (AB) method is an explicit linear multistep method that extrapolates from historical function values (Liu et al., 2022a). For order k , the AB formula is:

$$x_{n+1} = x_n + \Delta t \sum_{j=0}^{k-1} \beta_j f_{n-j}, \quad (5)$$

where β_j are coefficients derived from Lagrange interpolation (see Appendix A). Specifically, for the second-order case (AB2):

$$x_{n+1} = x_n + \frac{\Delta t}{2}(3f_n - f_{n-1}), \quad (6)$$



(a) Non-uniform Change Rate

(b) Skip Sensitivity

Figure 4. Feature dynamics vary across the diffusion process. (a) Initial and final phases exhibit rapid changes. (b) Approximation error grows with skip interval, especially in high-dynamics regions.

which achieves LTE of $\mathcal{O}(\Delta t^3)$, compared to $\mathcal{O}(\Delta t^2)$ for Euler. Crucially, AB directly combines historical function values without explicit derivative estimation, avoiding the instability of finite-difference approaches.

Adams-Moulton Corrector. While AB is efficient, its explicit nature can accumulate errors in high-dynamics regions. The Adams-Moulton (AM) method is an implicit corrector that includes the future value f_{n+1} :

$$x_{n+1} = x_n + \Delta t \sum_{j=-1}^{k-1} \gamma_j f_{n-j}, \quad (7)$$

where γ_{-1} corresponds to f_{n+1} . For the second-order case (AM2):

$$x_{n+1} = x_n + \frac{\Delta t}{12}(5f_{n+1} + 8f_n - f_{n-1}). \quad (8)$$

Combining AB as predictor and AM as corrector yields the Adams-Bashforth-Moulton (ABM) scheme (Karras et al., 2022), which first predicts \tilde{x}_{n+1} using AB, then evaluates $\tilde{f}_{n+1} = f_\theta(\tilde{x}_{n+1}, t_{n+1})$, and finally corrects using AM. While ABM achieves LTE of $\mathcal{O}(\Delta t^4)$ and improved stability, it requires one extra model call compared to AB alone. As shown in Figure 2(b), AB significantly reduces approximation error compared to naive reuse, and ABM further improves accuracy with lower accumulated drift.

To balance accuracy and efficiency, PrediT dynamically selects between AB and ABM based on the relative feature

Table 1. Comparison of visual quality and efficiency in text-to-image generation on FLUX.

Method	Acceleration				Image Reward \uparrow	CLIP Score \uparrow	Aesthetic Score \uparrow
	Latency(s) \downarrow	Speedup \uparrow	FLOP(T) \downarrow	Speedup \uparrow			
Original: 50 Steps	23.71	1.00 \times	3719.50	1.00 \times	0.9767	31.9448	6.7448
Δ -DiT($\mathcal{N} = 2$)	15.86	1.50 \times	1859.75	2.00 \times	0.9357	32.0211	6.5344
TeaCache($\tau = 0.4$)	12.31	1.92 \times	1438.92	2.58 \times	0.8710	31.7885	6.4400
ABM-Solver($\tau = 0.1$)	13.05	1.82 \times	952.22	3.90 \times	0.9378	<u>32.0804</u>	6.7260
Original: 25 Steps	11.58	2.05 \times	1859.75	2.00 \times	0.9467	31.6430	<u>6.7307</u>
Δ -DiT($\mathcal{N} = 3$)	11.50	2.06 \times	1264.63	2.94 \times	0.9385	31.8708	6.4825
TeaCache($\tau = 0.8$)	10.46	2.26 \times	899.32	4.13 \times	0.7933	31.6661	6.4048
FORA($\mathcal{N} = 3$)	8.73	2.71 \times	1264.63	2.94 \times	0.9715	32.0571	6.5433
AB-Cache($\mathcal{N} = 3$)	8.74	2.71 \times	1339.06	2.78 \times	0.9357	31.8480	6.6625
TaylorSeer($\mathcal{O} = 2, \mathcal{N} = 5$)	6.52	3.64 \times	892.68	4.17 \times	0.9676	31.9409	6.7439
FORA($\mathcal{N} = 4$)	6.90	3.44 \times	967.07	3.85 \times	0.9618	32.0679	6.5243
AB-Cache($\mathcal{N} = 4$)	6.49	3.65 \times	1026.76	3.62 \times	0.9308	31.8125	6.6681
TaylorSeer($\mathcal{O} = 2, \mathcal{N} = 6$)	6.02	3.94 \times	743.90	5.00 \times	<u>0.9761</u>	31.8897	6.7225
PrediT($\mathcal{O} = 2, \tau = 2$)	5.54	4.28 \times	743.92	5.00 \times	0.9773	32.1938	<u>6.7307</u>
PrediT($\mathcal{O} = 2, \tau = 2.5$)	4.28	5.54\times	639.77	5.81\times	0.9506	32.0696	6.7174

† **Bold** indicates the best result, underline indicates the second best. The same applies to the following tables.

change rate:

$$\delta_n = \frac{\|f_n - f_{n-1}\|_1}{\|f_n\|_1 + \epsilon}, \quad (9)$$

where ϵ is a small constant for numerical stability. ABM is applied in high-dynamics regions where accuracy is critical, while AB is used in smooth regions to maximize speedup.

Dynamic Step Modulation. As shown in Figure 4a, the model’s feature dynamics vary significantly along the diffusion trajectory, with initial and final phases exhibiting rapid changes. Figure 4b further reveals that skipping in high-dynamics regions incurs substantially larger feature deviation than in low-dynamics regions. Notably, even skipping multiple steps in smooth regions produces less error than a single skip in high-dynamics regions. Therefore, a fixed skip schedule cannot adapt to this variation (Karras et al., 2024). We compute the adaptive skip interval from the dynamics metric δ_n :

$$J = \left\lfloor \frac{\tau}{(\delta_n + \epsilon)^{1/(p+1)}} \right\rfloor, \quad (10)$$

where τ is the threshold parameter and p is the sensitivity exponent. The decision logic selects ABM without skipping when $\delta_n \geq \tau$, ABM with limited skipping when $\tau \cdot r \leq \delta_n < \tau$, and AB only with large skipping when $\delta_n < \tau \cdot r$, where r is the correction ratio. This ensures model calls focus on high-dynamics regions while maximizing skips in smooth regions.

Error Analysis. The total approximation error consists of discretization error from numerical integration, prediction error from polynomial extrapolation during skips, and accumulated drift from consecutive skips. Our framework

mitigates these by using higher-order AB/AM methods to reduce discretization error, adaptive skip interval to limit prediction error in curved regions, and ABM correction to reset accumulated drift when δ_n exceeds the threshold. Detailed error bounds are provided in Appendix B, and the complete algorithm is presented in Appendix C.

4. Experiments

4.1. Experimental Settings

Models, Datasets, and Solvers. We evaluate PrediT on three representative DiT-based models. For text-to-image generation, we use FLUX.1-dev (Labs et al., 2025) with 50 sampling steps and prompts from DiffusionDB (Wang et al., 2023). For text-to-video generation, we use Hunyuan-Video (Kong et al., 2024) with Rectified Flow (Liu et al., 2022b) solver, with prompts from VBench gallery (Zhang et al., 2025). For class-to-image generation, we use DiT-XL/2 (Peebles & Xie, 2023) with DDIM solver (Song et al., 2020a) on ImageNet (Deng et al., 2009) 256 \times 256.

Evaluation Metrics. For text-to-image, we report ImageReward (Xu et al., 2023) to measure human preference alignment, CLIP Score (Radford et al., 2021) for text-image consistency, and Aesthetic Score for visual appeal. For text-to-video, we use VBench (Zhang et al., 2025) for semantic quality and LPIPS (Zhang et al., 2018), SSIM (Wang et al., 2004), PSNR for frame-level fidelity compared to the original output. For class-to-image, we report FID and sFID (Heusel et al., 2017) for distribution similarity and Inception Score (IS) (Salimans et al., 2016) for sample quality and diversity. Detailed metric definitions are provided in Appendix D.



Figure 5. Visual quality comparison of different acceleration methods on FLUX. PrediT achieves higher acceleration while maintaining comparable visual quality.

Implementation Details. All experiments are conducted with FlashAttention (Dao et al., 2022) enabled. FLUX. 1 and HunyuanVideo are evaluated on a single NVIDIA A800 80GB GPU, while DiT-XL/2 uses an NVIDIA RTX 4090 24GB GPU. For FLUX.1, we generate 1024×1024 images. For HunyuanVideo, we test two settings: $544p \times 860p$ with 17 frames and $480p \times 640p$ with 45 frames. For DiT-XL/2, we generate 50K 256×256 images on ImageNet for FID evaluation. All baselines share the same solver, number of denoising steps, and CFG scale, unless otherwise specified by the original method.

4.2. Text-to-Image Generation

Quantitative Results. We evaluate PrediT on FLUX. 1 for text-to-image generation and compare with representative acceleration methods in Table 1. At comparable acceleration ratios, PrediT matches or improves generation quality across all metrics. Specifically, PrediT achieves superior speedup while attaining the highest ImageReward and CLIP Score, even surpassing the original 50-step baseline. When pushing to more aggressive acceleration, PrediT reaches up to $5.54 \times$

Table 2. Ablation study of predictor-corrector scheme and DSM on FLUX.1.

Method FLUX.1	Acceleration		Image Reward \uparrow	CLIP Score \uparrow
	Latency(s) \downarrow	Speedup \uparrow		
Original: 50 steps	23.71	1.00 \times	0.9767	31.9448
Only AB w/o DSM	6.49	3.65 \times	0.9308	31.8125
Only ABM w/o DSM	11.89	1.99 \times	0.9318	31.8634
Only AB + DSM	3.65	6.49 \times	0.9374	31.8534
Only ABM + DSM	6.15	3.86 \times	0.9671	32.1778
PrediT	5.54	4.28 \times	0.9773	32.1938

speedup with only marginal quality degradation. In contrast, reuse-based methods such as Δ -DiT and FORA suffer from noticeable quality drops at lower speedups. TeaCache achieves only $2.26 \times$ speedup but yields a lower ImageReward, significantly below the original. Prediction-based methods like TaylorSeer show improved quality retention but still fall short of PrediT at equivalent accelerations.

Visual Comparison. Figure 5 presents qualitative comparisons on FLUX. 1 (full prompts are provided in Appendix E, and more visual results are shown in Appendix F). Other acceleration methods exhibit visible artifacts including blurriness and loss of fine details, particularly in regions with complex textures. PrediT maintains visual fidelity comparable to the original model while achieving significantly higher acceleration, demonstrating the effectiveness of our principled prediction approach over naive feature reuse.

Ablation Study. To validate the effectiveness of our predictor-corrector scheme and Dynamic Step Modulation (DSM), we conduct ablation experiments on FLUX. 1 as shown in Table 2. Using only AB predictor without DSM achieves $3.65 \times$ speedup but with degraded ImageReward. Adding DSM to AB increases speedup to $6.49 \times$ while maintaining similar quality, demonstrating that adaptive step modulation allows larger skipping in smooth regions. Using ABM alone with DSM yields $3.86 \times$ speedup with improved quality, showing the benefit of the corrector in high-dynamics regions. The full PrediT framework, which dynamically selects between AB and ABM based on the dynamics metric, achieves an effective balance with $4.28 \times$ speedup and the highest ImageReward, validating the effectiveness of combining predictive feature forecasting with adaptive step modulation.

4.3. Text-to-Video Generation

Quantitative Results. We extend our evaluation to text-to-video generation on HunyuanVideo, testing two resolution settings as shown in Table 3. At $544p \times 860p$ with 17 frames, PrediT achieves $3.28 \times$ speedup while maintaining the highest VBench score and best visual metrics. Compared to other methods, PAB and TeaCache provide limited speedups with 50 sampling steps. Prediction-based methods face challenges in video generation; for example, TaylorSeer

Table 3. Comparison of visual quality and efficiency in text-to-video generation on HunyuanVideo on a single A800 GPU.

Settings	Method	Acceleration		Visual Quality			
		Latency(s) ↓	Speedup ↑	VBench(%) ↑	LPIPS ↓	SSIM ↑	PSNR ↑
544p×860p, 17frames	Original: 50 Steps	76.71	1.00×	82.08	0.0000	1.000	∞
	PAB($\mathcal{N} = 8$)	66.21	1.16×	80.81	0.1433	0.8370	27.41
	TeaCache($\tau = 0.14$)	57.71	1.33×	82.18	0.1466	0.8536	25.64
	Original: 25 Steps	40.29	1.90×	81.51	0.1973	0.8196	23.17
	ProfilingDiT($\mathcal{N} = 6$)	44.60	1.72×	80.33	0.2610	0.6662	18.77
	TaylorSeer($\mathcal{O} = 1, \mathcal{N} = 4$)	39.30	1.95×	82.05	0.4021	0.5526	15.33
	AB-Cache($\mathcal{N} = 3$)	32.14	2.39×	82.36	0.1587	0.8512	24.67
	PrediT($\mathcal{O} = 2, \tau = 2$)	27.21	2.81×	82.45	0.1329	0.8693	<u>25.81</u>
	PrediT($\mathcal{O} = 3, \tau = 2.5$)	23.36	3.28×	82.36	0.1429	0.8616	25.77
	480p×640p, 45frames	Original: 50 Steps	117.43	1.00×	80.12	0.0000	1.000
PAB($\mathcal{N} = 8$)		95.14	1.23×	78.45	0.1712	0.7969	25.67
TeaCache($\tau = 0.14$)		77.86	1.51×	80.05	0.1701	0.8036	23.48
Original: 25 Steps		62.14	1.89×	79.76	0.2221	0.7599	20.95
AB-Cache($\mathcal{N} = 3$)		49.29	2.38×	79.89	0.1801	0.7995	22.68
PrediT($\mathcal{O} = 2, \tau = 2$)		41.29	2.84×	80.14	0.1401	0.8345	<u>24.25</u>
PrediT($\mathcal{O} = 3, \tau = 2.5$)		36.14	3.24×	80.08	0.1513	0.8280	24.06

† ProfilingDiT and TaylorSeer can only generate up to 17 frames at 544p×860p resolution on a single A800 GPU, and run OOM at 480p×640p with 45 frames.

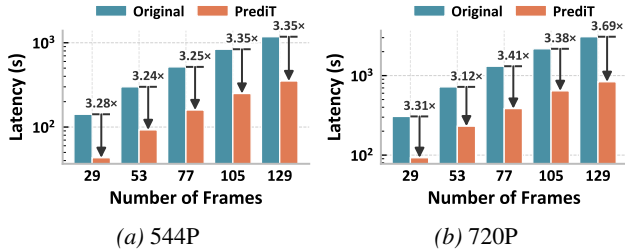


Figure 6. Latency comparison between the original method and PrediT on HunyuanVideo at 544P and 720P resolutions across different frame counts.

achieves comparable speedup but with degraded visual quality, indicating accumulated prediction errors across video frames. AB-Cache shows better quality retention but PrediT still outperforms it in both acceleration and visual fidelity. At 480p×640p with 45 frames, the computational challenge increases, yet PrediT maintains consistent acceleration with the best VBench score. Notably, ProfilingDiT and TaylorSeer encounter out-of-memory (OOM) errors at this setting, highlighting the memory efficiency of our approach. Detailed memory analysis is provided in Appendix G.

Scaling Analysis. Figure 6 illustrates the latency scaling behavior across different frame counts at 544P and 720P resolutions. The original method exhibits near-linear latency growth with increasing frames, becoming prohibitive for longer video generation. PrediT consistently reduces latency across all configurations, with the acceleration ratio remaining stable as frame count increases. This demonstrates that our dynamic step modulation adapts effectively

to the temporal structure of video diffusion, maintaining efficient inference regardless of video length.

Visual Comparison. Figure 7 presents visual comparisons on HunyuanVideo. Other acceleration methods suffer from noticeable quality degradation, including blurriness and loss of fine details in both spatial and temporal dimensions. PrediT preserves the visual quality of the original model, with sharp details and consistent motion across frames, validating the effectiveness of our predictor-corrector scheme.

4.4. Class-to-Image Generation

Quantitative Results. In Table 4, we evaluate PrediT on DiT-XL/2 for class-conditional ImageNet generation, comparing with existing acceleration methods under both 50-step and 70-step DDIM sampling. Notably, Learning-to-Cache (L2C) (Ma et al., 2024a) learns to conduct caching in a dynamic manner for diffusion transformers, which is not training-free. At 50 steps, PrediT achieves 2.12× speedup while improving FID from 2.28 to 2.24, demonstrating that our method can simultaneously accelerate inference and enhance generation quality. This improvement stems from the reduced discretization error of our higher-order prediction scheme. In comparison, FORA achieves 2.03× speedup but degrades FID to 3.52, and L2C provides only 1.25× acceleration. At 70 steps, PrediT maintains consistent performance with 2.48× speedup and FID of 2.24. Notably, TaylorSeer exhibits severe quality collapse at 70 steps with FID degrading to 10.12, indicating numerical instability in its Taylor series extrapolation over longer sampling trajectories. PrediT avoids this issue through the stability properties



Figure 7. Visual quality comparison of different acceleration methods on HunyuanVideo. Other acceleration methods suffer from blurriness or loss of details, while PrediT maintains comparable visual quality with higher acceleration.

Table 4. Comparison of visual quality and efficiency in class-to-image generation on DiT-XL/2.

Method	Steps	Latency(s) ↓	Speedup ↑	FID ↓	sFID ↓	IS ↑
DDIM	50	0.569	1.00×	2.28	4.25	242.26
L2C _{0.5}	50	0.455	1.25×	2.39	4.40	235.75
FORA ₂	50	0.331	1.72×	2.73	4.90	234.57
FORA ₃	50	0.280	2.03×	3.52	6.39	226.18
TaylorSeer ₃	50	0.409	1.39×	2.41	4.69	235.83
PrediT _{1,0.1} ⁴	50	0.309	1.84×	2.23	<u>4.60</u>	240.10
PrediT _{1,0.3} ⁴	50	0.268	2.12×	<u>2.24</u>	4.78	<u>239.55</u>
DDIM	70	0.779	1.00×	2.21	4.29	243.92
FORA ₂	70	0.449	1.73×	2.43	4.59	<u>244.19</u>
FORA ₃	70	0.335	2.33×	2.85	5.40	241.42
TaylorSeer ₃	70	0.553	1.41×	10.12	16.35	175.62
PrediT _{1,0.1} ⁴	70	0.356	2.19×	2.15	<u>4.61</u>	245.15
PrediT _{1,0.3} ⁴	70	0.314	2.48×	<u>2.24</u>	4.77	239.54

of Adams methods and adaptive corrector activation.

Quality-Speedup Trade-off. Figure 8 visualizes the quality-speedup trade-off between DDIM and PrediT with different predictor orders. Higher-order predictors achieve better FID and IS at the cost of slightly reduced speedup. Notably, PrediT with $\mathcal{O} = 4$ surpasses the DDIM baseline in both FID and IS while still providing acceleration, demonstrating that our method can improve quality while accelerating inference. Suggesting that users choose the parameters flexibly. Additional ablation studies with various hyperparameter configurations are provided in Appendix H.

5. Conclusion

In this paper, we presented PrediT, a training-free acceleration framework for DiTs that formulates feature prediction

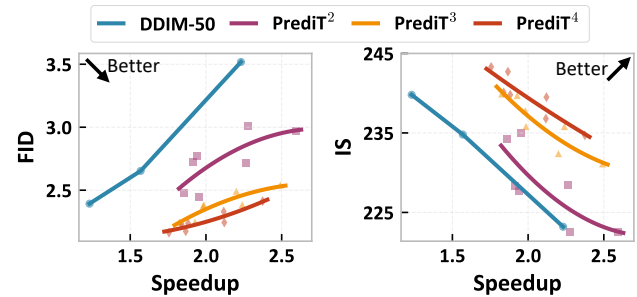


Figure 8. Quality-speedup trade-off on DiT-XL/2. PrediT achieves better quality at a higher speedup compared to the original model.

as a linear multistep problem. Observing that model outputs evolve smoothly along the diffusion trajectory, we moved beyond naive feature reuse to principled prediction. Our framework employs the Adams-Bashforth predictor to extrapolate future model outputs from historical information, and an Adams-Moulton corrector that activates in high-dynamics regions to prevent error accumulation. The dynamic step modulation mechanism adaptively adjusts the prediction horizon based on the relative feature change rate, enabling aggressive skipping in smooth regions while maintaining accuracy in high-dynamics regions. Experiments across DiT-based models demonstrate the effectiveness of PrediT. Future work includes extending our framework to emerging architectures such as Mixture-of-Experts DiT models and exploring applications in interactive generation scenarios.

Impact Statements

This paper presents work whose goal is to advance the field of machine learning, particularly in efficient inference for generative models. The proposed PrediT framework has several positive societal implications:

- **Environmental Efficiency:** By reducing model inference latency while maintaining generation quality, our method directly lowers the energy consumption and carbon footprint of running large-scale diffusion models for image and video generation.
- **Democratization of Access:** Our method introduces minimal memory overhead, enabling high-resolution video generation on a consumer-grade GPU without out-of-memory errors. This broadens access to advanced generative tools for researchers and creators with limited computational resources.

References

- Blattmann, A., Dockhorn, T., Kulal, S., Mendeleevitch, D., Kilian, M., Lorenz, D., Levi, Y., English, Z., Voleti, V., Letts, A., et al. Stable video diffusion: Scaling latent video diffusion models to large datasets. *arXiv preprint arXiv:2311.15127*, 2023.
- Butcher, J. C. *Numerical methods for ordinary differential equations*. John Wiley & Sons, 2016.
- Cao, Y., Li, S., Liu, Y., Yan, Z., Dai, Y., Yu, P., and Sun, L. A survey of ai-generated content (aigc). *ACM Computing Surveys*, 57(5):1–38, 2025.
- Chen, H., Xia, M., He, Y., Zhang, Y., Cun, X., Yang, S., Xing, J., Liu, Y., Chen, Q., Wang, X., et al. Videocrafter1: Open diffusion models for high-quality video generation. *arXiv preprint arXiv:2310.19512*, 2023a.
- Chen, H., Zhang, Y., Cun, X., Xia, M., Wang, X., Weng, C., and Shan, Y. Videocrafter2: Overcoming data limitations for high-quality video diffusion models. In *Proceedings of the IEEE/CVF Conference on Computer Vision and Pattern Recognition*, pp. 7310–7320, 2024a.
- Chen, J., Yu, J., Ge, C., Yao, L., Xie, E., Wu, Y., Wang, Z., Kwok, J., Luo, P., Lu, H., et al. Pixart- α : Fast training of diffusion transformer for photorealistic text-to-image synthesis. *arXiv preprint arXiv:2310.00426*, 2023b.
- Chen, J., Ge, C., Xie, E., Wu, Y., Yao, L., Ren, X., Wang, Z., Luo, P., Lu, H., and Li, Z. Pixart- σ : Weak-to-strong training of diffusion transformer for 4k text-to-image generation. In *European Conference on Computer Vision*, pp. 74–91. Springer, 2024b.
- Chen, P., Shen, M., Ye, P., Cao, J., Tu, C., Bouganis, C.-S., Zhao, Y., and Chen, T. δ -dit: A training-free acceleration method tailored for diffusion transformers. *arXiv preprint arXiv:2406.01125*, 2024c.
- Croitoru, F.-A., Hondru, V., Ionescu, R. T., and Shah, M. Diffusion models in vision: A survey. *IEEE transactions on pattern analysis and machine intelligence*, 45(9): 10850–10869, 2023.
- Dao, T., Fu, D. Y., Ermon, S., Rudra, A., and Ré, C. FlashAttention: Fast and memory-efficient exact attention with IO-awareness. In *Advances in neural information processing systems*, 2022.
- Deng, J., Dong, W., Socher, R., Li, L.-J., Li, K., and Fei-Fei, L. Imagenet: A large-scale hierarchical image database. In *2009 IEEE conference on computer vision and pattern recognition*, pp. 248–255. Ieee, 2009.
- Dhariwal, P. and Nichol, A. Diffusion models beat gans on image synthesis. In *Advances in neural information processing systems*, volume 34, pp. 8780–8794, 2021.
- Esser, P., Kulal, S., Blattmann, A., Entezari, R., Müller, J., Saini, H., Levi, Y., Lorenz, D., Sauer, A., Boesel, F., et al. Scaling rectified flow transformers for high-resolution image synthesis. In *Forty-first international conference on machine learning*, 2024.
- Fui-Hoon Nah, F., Zheng, R., Cai, J., Siau, K., and Chen, L. Generative ai and chatgpt: Applications, challenges, and ai-human collaboration. *Journal of information technology case and application research*, 25(3):277–304, 2023.
- Hairer, E., Wanner, G., and Nørsett, S. P. *Solving ordinary differential equations I: Nonstiff problems*. Springer, 1993.
- Heusel, M., Ramsauer, H., Unterthiner, T., Nessler, B., and Hochreiter, S. Gans trained by a two time-scale update rule converge to a local nash equilibrium. In *Advances in neural information processing systems*, volume 30, 2017.
- Ho, J., Jain, A., and Abbeel, P. Denoising diffusion probabilistic models. In *Advances in neural information processing systems*, volume 33, pp. 6840–6851, 2020.
- Karras, T., Aittala, M., Aila, T., and Laine, S. Elucidating the design space of diffusion-based generative models. In *Advances in neural information processing systems*, volume 35, pp. 26565–26577, 2022.
- Karras, T., Aittala, M., Lehtinen, J., Hellsten, J., Aila, T., and Laine, S. Analyzing and improving the training dynamics of diffusion models. In *Proceedings of the IEEE/CVF Conference on Computer Vision and Pattern Recognition*, pp. 24174–24184, 2024.

- Kong, W., Tian, Q., Zhang, Z., Min, R., Dai, Z., Zhou, J., Xiong, J., Li, X., Wu, B., Zhang, J., et al. Hunyuan-video: A systematic framework for large video generative models. *arXiv preprint arXiv:2412.03603*, 2024.
- Labs, B. F., Batifol, S., Blattmann, A., Boesel, F., Consul, S., Diagne, C., Dockhorn, T., English, J., English, Z., Esser, P., et al. Flux. 1 kontext: Flow matching for in-context image generation and editing in latent space. *arXiv preprint arXiv:2506.15742*, 2025.
- Li, X., Liu, Y., Lian, L., Yang, H., Dong, Z., Kang, D., Zhang, S., and Keutzer, K. Q-diffusion: Quantizing diffusion models. In *Proceedings of the IEEE/CVF International Conference on Computer Vision*, pp. 17535–17545, 2023.
- Lipman, Y., Chen, R. T., Ben-Hamu, H., Nickel, M., and Le, M. Flow matching for generative modeling. *arXiv preprint arXiv:2210.02747*, 2022.
- Liu, F., Zhang, S., Wang, X., Wei, Y., Qiu, H., Zhao, Y., Zhang, Y., Ye, Q., and Wan, F. Timestep embedding tells: It’s time to cache for video diffusion model. In *Proceedings of the Computer Vision and Pattern Recognition Conference*, pp. 7353–7363, 2025a.
- Liu, J., Geddes, J., Guo, Z., Jiang, H., and Nandwana, M. K. Smoothcache: A universal inference acceleration technique for diffusion transformers. In *Proceedings of the Computer Vision and Pattern Recognition Conference*, pp. 3229–3238, 2025b.
- Liu, J., Wang, X., Lin, Y., Wang, Z., Wang, P., Cai, P., Zhou, Q., Yan, Z., Yan, Z., Shi, Z., et al. A survey on cache methods in diffusion models: Toward efficient multi-modal generation. *arXiv preprint arXiv:2510.19755*, 2025c.
- Liu, J., Zou, C., Lyu, Y., Chen, J., and Zhang, L. From reusing to forecasting: Accelerating diffusion models with taylorseers. *arXiv preprint arXiv:2503.06923*, 2025d.
- Liu, L., Ren, Y., Lin, Z., and Zhao, Z. Pseudo numerical methods for diffusion models on manifolds. *arXiv preprint arXiv:2202.09778*, 2022a.
- Liu, X., Gong, C., and Liu, Q. Flow straight and fast: Learning to generate and transfer data with rectified flow. *arXiv preprint arXiv:2209.03003*, 2022b.
- Liu, Y., Zhang, K., Li, Y., Yan, Z., Gao, C., Chen, R., Yuan, Z., Huang, Y., Sun, H., Gao, J., et al. Sora: A review on background, technology, limitations, and opportunities of large vision models. *arXiv preprint arXiv:2402.17177*, 2024.
- Lu, C., Zhou, Y., Bao, F., Chen, J., Li, C., and Zhu, J. Dpm-solver: A fast ode solver for diffusion probabilistic model sampling in around 10 steps. In *Advances in neural information processing systems*, volume 35, pp. 5775–5787, 2022.
- Lu, C., Zhou, Y., Bao, F., Chen, J., Li, C., and Zhu, J. Dpm-solver++: Fast solver for guided sampling of diffusion probabilistic models. *Machine Intelligence Research*, pp. 1–22, 2025.
- Ma, X., Fang, G., Bi Mi, M., and Wang, X. Learning-to-cache: Accelerating diffusion transformer via layer caching. In *Advances in Neural Information Processing Systems*, volume 37, pp. 133282–133304, 2024a.
- Ma, X., Fang, G., and Wang, X. Deepcache: Accelerating diffusion models for free. In *Proceedings of the IEEE/CVF conference on computer vision and pattern recognition*, pp. 15762–15772, 2024b.
- Ma, X., Liu, Y., Liu, Y., Wu, X., Zheng, M., Wang, Z., Lim, S.-N., and Yang, H. Model reveals what to cache: Profiling-based feature reuse for video diffusion models. In *Proceedings of the IEEE/CVF International Conference on Computer Vision (ICCV)*, pp. 17150–17159, October 2025a.
- Ma, Y., Di, D., Liu, X., Chen, X., Fan, L., Chen, W., and Su, T. Adams bashforth moulton solver for inversion and editing in rectified flow. *arXiv preprint arXiv:2503.16522*, 2025b.
- Meng, C., Rombach, R., Gao, R., Kingma, D., Ermon, S., Ho, J., and Salimans, T. On distillation of guided diffusion models. In *Proceedings of the IEEE/CVF conference on computer vision and pattern recognition*, pp. 14297–14306, 2023.
- Peebles, W. and Xie, S. Scalable diffusion models with transformers. In *Proceedings of the IEEE/CVF international conference on computer vision*, pp. 4195–4205, 2023.
- Radford, A., Kim, J. W., Hallacy, C., Ramesh, A., Goh, G., Agarwal, S., Sastry, G., Askell, A., Mishkin, P., Clark, J., et al. Learning transferable visual models from natural language supervision. In *International conference on machine learning*, pp. 8748–8763. PmLR, 2021.
- Ramesh, A., Dhariwal, P., Nichol, A., Chu, C., and Chen, M. Hierarchical text-conditional image generation with clip latents. *arXiv preprint arXiv:2204.06125*, 1(2):3, 2022.
- Rombach, R., Blattmann, A., Lorenz, D., Esser, P., and Ommer, B. High-resolution image synthesis with latent diffusion models. In *Proceedings of the IEEE/CVF conference on computer vision and pattern recognition*, pp. 10684–10695, 2022.

- Salimans, T. and Ho, J. Progressive distillation for fast sampling of diffusion models. *arXiv preprint arXiv:2202.00512*, 2022.
- Salimans, T., Goodfellow, I., Zaremba, W., Cheung, V., Radford, A., and Chen, X. Improved techniques for training gans. In *Advances in neural information processing systems*, volume 29, 2016.
- Selvaraju, P., Ding, T., Chen, T., Zharkov, I., and Liang, L. Fora: Fast-forward caching in diffusion transformer acceleration. *arXiv preprint arXiv:2407.01425*, 2024.
- Shang, Y., Yuan, Z., Xie, B., Wu, B., and Yan, Y. Post-training quantization on diffusion models. In *Proceedings of the IEEE/CVF conference on computer vision and pattern recognition*, pp. 1972–1981, 2023.
- Song, J., Meng, C., and Ermon, S. Denoising diffusion implicit models. *arXiv preprint arXiv:2010.02502*, 2020a.
- Song, Y., Sohl-Dickstein, J., Kingma, D. P., Kumar, A., Ermon, S., and Poole, B. Score-based generative modeling through stochastic differential equations. *arXiv preprint arXiv:2011.13456*, 2020b.
- Wang, Z., Bovik, A. C., Sheikh, H. R., and Simoncelli, E. P. Image quality assessment: from error visibility to structural similarity. *IEEE transactions on image processing*, 13(4):600–612, 2004.
- Wang, Z. J., Montoya, E., Munechika, D., Yang, H., Hoover, B., and Chau, D. H. Diffusiondb: A large-scale prompt gallery dataset for text-to-image generative models. In *Proceedings of the 61st annual meeting of the association for computational linguistics*, pp. 893–911, 2023.
- Xu, J., Liu, X., Wu, Y., Tong, Y., Li, Q., Ding, M., Tang, J., and Dong, Y. Imagereward: learning and evaluating human preferences for text-to-image generation. In *Proceedings of the 37th International Conference on Neural Information Processing Systems*, pp. 15903–15935, 2023.
- Yang, L., Zhang, Z., Song, Y., Hong, S., Xu, R., Zhao, Y., Zhang, W., Cui, B., and Yang, M.-H. Diffusion models: A comprehensive survey of methods and applications. *ACM computing surveys*, 56(4):1–39, 2023.
- Yu, Z., Zou, Z., Shao, G., Zhang, C., Xu, S., Huang, J., Zhao, F., Cun, X., and Zhang, W. Ab-cache: Training-free acceleration of diffusion models via adams-bashforth cached feature reuse. In *Proceedings of the 33rd ACM International Conference on Multimedia*, pp. 10408–10417, 2025.
- Zhang, F., Tian, S., Huang, Z., Qiao, Y., and Liu, Z. Evaluation agent: Efficient and promptable evaluation framework for visual generative models. In *Annual Meeting of the Association for Computational Linguistics (ACL)*, 2025, 2025.
- Zhang, R., Isola, P., Efros, A. A., Shechtman, E., and Wang, O. The unreasonable effectiveness of deep features as a perceptual metric. In *Proceedings of the IEEE conference on computer vision and pattern recognition*, pp. 586–595, 2018.
- Zhao, X., Jin, X., Wang, K., and You, Y. Real-time video generation with pyramid attention broadcast. *arXiv preprint arXiv:2408.12588*, 2024.
- Zheng, Z., Peng, X., Yang, T., Shen, C., Li, S., Liu, H., Zhou, Y., Li, T., and You, Y. Open-sora: Democratizing efficient video production for all. *arXiv preprint arXiv:2412.20404*, 2024.

A. Adams Method Coefficients

A.1. Derivation of Second-Order Adams-Bashforth (AB2)

The Adams-Bashforth method approximates the integral $\int_{t_n}^{t_{n+1}} f(x(s), s) ds$ by constructing a Lagrange interpolating polynomial through historical function values. For the second-order case (AB2), we use two points (t_n, f_n) and (t_{n-1}, f_{n-1}) .

The Lagrange interpolating polynomial is:

$$P(s) = f_n \cdot \frac{s - t_{n-1}}{t_n - t_{n-1}} + f_{n-1} \cdot \frac{s - t_n}{t_{n-1} - t_n} = f_n \cdot \frac{s - t_{n-1}}{h} - f_{n-1} \cdot \frac{s - t_n}{h}, \quad (11)$$

where $h = \Delta t$ is the uniform step size. Integrating from t_n to t_{n+1} :

$$\int_{t_n}^{t_{n+1}} P(s) ds = \frac{f_n}{h} \int_{t_n}^{t_{n+1}} (s - t_{n-1}) ds - \frac{f_{n-1}}{h} \int_{t_n}^{t_{n+1}} (s - t_n) ds \quad (12)$$

$$= \frac{f_n}{h} \left[\frac{(s - t_{n-1})^2}{2} \right]_{t_n}^{t_{n+1}} - \frac{f_{n-1}}{h} \left[\frac{(s - t_n)^2}{2} \right]_{t_n}^{t_{n+1}} \quad (13)$$

$$= \frac{f_n}{h} \cdot \frac{(2h)^2 - h^2}{2} - \frac{f_{n-1}}{h} \cdot \frac{h^2}{2} = \frac{3h}{2} f_n - \frac{h}{2} f_{n-1}. \quad (14)$$

Thus, the AB2 formula is:

$$x_{n+1} = x_n + \frac{h}{2}(3f_n - f_{n-1}), \quad (15)$$

with coefficients $\beta_0 = \frac{3}{2}$ and $\beta_1 = -\frac{1}{2}$.

A.2. Derivation of Second-Order Adams-Moulton (AM2)

The Adams-Moulton method includes the future value f_{n+1} in the interpolation, making it implicit. For the second-order case (AM2), we construct a polynomial through three points (t_{n+1}, f_{n+1}) , (t_n, f_n) , and (t_{n-1}, f_{n-1}) :

$$P(s) = f_{n+1}L_{-1}(s) + f_nL_0(s) + f_{n-1}L_1(s), \quad (16)$$

where $L_j(s)$ are the Lagrange basis polynomials. After computing the integrals:

$$\int_{t_n}^{t_{n+1}} L_{-1}(s) ds = \frac{5h}{12}, \quad \int_{t_n}^{t_{n+1}} L_0(s) ds = \frac{8h}{12}, \quad \int_{t_n}^{t_{n+1}} L_1(s) ds = -\frac{h}{12}. \quad (17)$$

Thus, the AM2 formula is:

$$x_{n+1} = x_n + \frac{h}{12}(5f_{n+1} + 8f_n - f_{n-1}), \quad (18)$$

with coefficients $\gamma_{-1} = \frac{5}{12}$, $\gamma_0 = \frac{8}{12}$, and $\gamma_1 = -\frac{1}{12}$.

A.3. Higher-Order Coefficients

Following the same derivation procedure, we obtain coefficients for higher-order methods. Table 5 and Table 6 summarize the coefficients and local truncation errors (LTE) for orders 1–4.

Table 5. Adams-Bashforth coefficients and local truncation errors.

Order	β_0	β_1	β_2	β_3	LTE
AB1	1	–	–	–	$\frac{1}{2}h^2 f''$
AB2	$\frac{3}{2}$	$-\frac{1}{2}$	–	–	$\frac{5}{12}h^3 f'''$
AB3	$\frac{23}{12}$	$-\frac{16}{12}$	$\frac{5}{12}$	–	$\frac{9}{24}h^4 f^{(4)}$
AB4	$\frac{55}{24}$	$-\frac{59}{24}$	$\frac{37}{24}$	$-\frac{9}{24}$	$\frac{251}{720}h^5 f^{(5)}$

Note that AM of the same order has a smaller LTE coefficient than AB, providing improved accuracy at the cost of requiring f_{n+1} .

Table 6. Adams-Moulton coefficients and local truncation errors.

Order	γ_{-1}	γ_0	γ_1	γ_2	γ_3	LTE
AM1	1	—	—	—	—	$-\frac{1}{2}h^2 f''$
AM2	$\frac{5}{12}$	$\frac{8}{12}$	$-\frac{1}{12}$	—	—	$-\frac{1}{24}h^3 f'''$
AM3	$\frac{9}{24}$	$\frac{19}{24}$	$-\frac{5}{24}$	$\frac{1}{24}$	—	$-\frac{19}{720}h^4 f^{(4)}$
AM4	$\frac{251}{720}$	$\frac{646}{720}$	$-\frac{264}{720}$	$\frac{106}{720}$	$-\frac{19}{720}$	$-\frac{3}{160}h^5 f^{(5)}$

B. Error Analysis

B.1. Discretization Error

For an ODE $\dot{x} = f(x, t)$ with exact solution $x(t)$, the local truncation error (LTE) of a numerical method measures the error introduced in a single step assuming exact previous values.

Proposition B.1 (AB Local Truncation Error). *The Adams-Bashforth method of order k has LTE:*

$$\tau_n^{AB} = C_k h^{k+1} f^{(k)}(\xi) + \mathcal{O}(h^{k+2}), \quad (19)$$

where C_k is a constant depending on k , and $\xi \in [t_n, t_{n+1}]$.

The global error after N steps is bounded by:

$$\|x_N - x(t_N)\| \leq \frac{e^{LT} - 1}{L} \max_n \|\tau_n\| = \mathcal{O}(h^k), \quad (20)$$

where L is the Lipschitz constant of f and T is the total integration time.

B.2. Prediction Error During Skips

When skipping model calls, we use AB to predict f_{n+1} from history:

$$\hat{f}_{n+1} = \sum_{j=0}^{k-1} \alpha_j f_{n-j}, \quad (21)$$

where α_j are extrapolation coefficients. The prediction error is:

$$\epsilon_{\text{pred}} = \|f_{n+1} - \hat{f}_{n+1}\| \approx \mathcal{O}(h^k \|f^{(k)}\|). \quad (22)$$

This error depends on the local curvature of the trajectory. Our dynamics metric δ_n approximates the first derivative, providing a proxy for curvature.

B.3. Error Accumulation and Mitigation

When J consecutive steps are skipped, errors accumulate:

$$\epsilon_{\text{acc}}(J) \approx \sum_{i=1}^J \epsilon_{\text{pred}}(i) \cdot (1 + Lh)^{J-i}. \quad (23)$$

The exponential factor $(1 + Lh)^{J-i}$ reflects error propagation through the ODE. Our framework mitigates this through:

1. **Adaptive skip interval:** When δ_n is large, J is automatically reduced via Equation (10).
2. **ABM correction:** When $\delta_n \geq \tau$, we invoke ABM which evaluates the true f_{n+1} , resetting the prediction error to the discretization error of AM.

3. **Threshold-based switching:** The correction ratio r creates a buffer zone where ABM is used even for moderate dynamics.

Proposition B.2 (Error Bound with Dynamic Step Modulation). *Under the assumption that $\|f^{(k)}\| \leq M$ and with threshold τ chosen such that $\delta_n < \tau$ implies $\|f'\| \leq \tau\|f\|$, the accumulated error over a trajectory satisfies:*

$$\|\epsilon_{total}\| \leq C_1 h^k + C_2 \tau J_{\max} + C_3 N_{ABM}, \quad (24)$$

where J_{\max} is the maximum allowed skip interval and N_{ABM} is the number of ABM corrections that reset the accumulated drift.

This shows that the error is controlled by the interplay between the method order k , the threshold τ , and the frequency of corrections.

C. Algorithm Pseudocode

Algorithm 1 PrediT: Predictive Diffusion Transformer Inference

Require: Noise x_1 , timesteps $\{t_n\}_{n=0}^N$, model f_θ , order k , threshold τ , ratio r
Initialize history buffer $\mathcal{H} \leftarrow \emptyset$, skip counter $J \leftarrow 0$
for $n = 0$ to $N - 1$ **do**
 $\Delta t \leftarrow t_{n+1} - t_n$
 if $J > 0$ **then**
 $x \leftarrow x + \text{AB}_k(\Delta t, \mathcal{H})$ // Skip: use cached history
 $J \leftarrow J - 1$
 else
 $f_n \leftarrow f_\theta(x, t_n)$ // Compute model output
 $\delta_n \leftarrow \|f_n - f_{n-1}\|_1 / (\|f_n\|_1 + \epsilon)$ // Dynamics metric
 if $\delta_n \geq \tau$ **then**
 $x \leftarrow \text{ABM}_k(x, \Delta t, f_n, \mathcal{H}, f_\theta)$ // Corrected by ABM
 else if $\delta_n \geq \tau \cdot r$ **then**
 $x \leftarrow \text{ABM}_k(x, \Delta t, f_n, \mathcal{H}, f_\theta)$, $J \leftarrow \text{ComputeSkip}(\delta_n, \tau)$ // Corrected by ABM with dynamic step modulation
 else
 $x \leftarrow x + \text{AB}_k(\Delta t, [f_n] \cup \mathcal{H})$, $J \leftarrow \text{ComputeSkip}(\delta_n, \tau)$ // Predicted by AB with dynamic step modulation
 end if
 Update $\mathcal{H} \leftarrow [f_n] \cup \mathcal{H}$
 end if
 end for
return x

D. Evaluation Metrics

D.1. Text-to-Image Metrics

ImageReward. ImageReward measures the alignment between generated images and human preferences. It is trained on human preference data to predict which image better matches the given text prompt:

$$\text{ImageReward}(x, c) = f_\phi(x, c), \quad (25)$$

where x is the generated image, c is the text prompt, and f_ϕ is the reward model trained on human annotations.

CLIP Score. CLIP Score evaluates the semantic consistency between the generated image and the input text prompt using a pretrained CLIP model:

$$\text{CLIPScore}(x, c) = \max(100 \cdot \cos(E_I(x), E_T(c)), 0), \quad (26)$$

where E_I and E_T are the image and text encoders of CLIP, and $\cos(\cdot, \cdot)$ denotes cosine similarity.

Aesthetic Score. Aesthetic Score predicts the visual appeal of generated images using a model trained on human aesthetic ratings:

$$\text{AestheticScore}(x) = g_\psi(E_I(x)), \quad (27)$$

where g_ψ is a linear regressor trained on the Aesthetic Visual Analysis (AVA) dataset aesthetic annotations.

D.2. Text-to-Video Metrics

VBench. VBench is a comprehensive benchmark that evaluates video generation across multiple dimensions, including subject consistency, background consistency, motion smoothness, aesthetic quality, and imaging quality. The overall score is a weighted combination of these sub-metrics.

LPIPS. Learned Perceptual Image Patch Similarity measures perceptual similarity between frames:

$$\text{LPIPS}(x, y) = \sum_l \frac{1}{H_l W_l} \sum_{h,w} \|w_l \odot (\hat{\phi}_l^{hw}(x) - \hat{\phi}_l^{hw}(y))\|_2^2, \quad (28)$$

where $\hat{\phi}_l$ are normalized activations from layer l of a pretrained network and w_l are learned weights.

SSIM. Structural Similarity Index measures the structural similarity between two images:

$$\text{SSIM}(x, y) = \frac{(2\mu_x\mu_y + c_1)(2\sigma_{xy} + c_2)}{(\mu_x^2 + \mu_y^2 + c_1)(\sigma_x^2 + \sigma_y^2 + c_2)}, \quad (29)$$

where μ_x, μ_y are local means, σ_x, σ_y are standard deviations, σ_{xy} is the covariance, and c_1, c_2 are stability constants.

PSNR. Peak Signal-to-Noise Ratio measures the reconstruction quality:

$$\text{PSNR}(x, y) = 10 \cdot \log_{10} \left(\frac{R^2}{\text{MSE}(x, y)} \right), \quad (30)$$

where R is the maximum possible pixel value, and MSE is the mean squared error.

D.3. Class-to-Image Metrics

FID. Fréchet Inception Distance measures the similarity between the distributions of generated and real images:

$$\text{FID} = \|\mu_r - \mu_g\|^2 + \text{Tr}(\Sigma_r + \Sigma_g - 2(\Sigma_r \Sigma_g)^{1/2}), \quad (31)$$

where (μ_r, Σ_r) and (μ_g, Σ_g) are the mean and covariance of Inception features for real and generated images.

sFID. Spatial FID computes FID on spatial feature maps rather than pooled features, better capturing spatial structure.

Inception Score. Inception Score evaluates both quality and diversity of generated samples:

$$\text{IS} = \exp(\mathbb{E}_x[D_{KL}(p(y|x)||p(y))]), \quad (32)$$

where $p(y|x)$ is the conditional class distribution from an Inception classifier and $p(y) = \mathbb{E}_x[p(y|x)]$ is the marginal distribution. Higher IS indicates both confident class predictions and diverse class coverage.

E. Text-to-Image Prompt

The prompts used for the visual comparisons in Figure 5 are listed below:

1. **Column 1:** ["rat with bandages on bandaged arms holding wakizashi, highly detailed, d & d, fantasy, highly detailed, digital painting, trending on artstation, concept art, sharp focus, illustration, global illumination, shaded, art by artgerm and greg rutkowski and fuji choko and viktorija gavrilenko and hoang lap"]

Table 7. Memory Usage (MB) on Different Resolutions and Frames using A800 80GB.

Method	480p×640p×45f	480p×640p×65f	544p×860p×17f	544p×860p×65f	720p×1280p×129f
Original	44295	45949	43131	49477	74465
PrediT	44819	46313	44043	49715	74525
PAB	79831	OOM	55045	OOM	OOM
TeaCache	48619	51499	48227	53319	80083
ProfilingDiT	OOM	OOM	57237	OOM	OOM
TaylorSeer	OOM	OOM	61557	OOM	OOM

- Column 2:** [“anna from frozen — — fine detail!! anime!! realistic shaded lighting!!, directional lighting 2 d poster by ilya kuvshinov, magali villeneuve, artgerm, jeremy lipkin and michael garmash and rob rey”]
- Column 3:** [“a boy holding on to a dying old dog connecting him to his childhood”]
- Column 4:** [“a beautiful ultradetailed anime illustration of unknown backroom level nature by bjarke ingels, landscape sunlight laser studio ghibli infrared cyberpunk at night synthwave tokyo vaporwave neon noir magic realism, archdaily, wallpaper, highly detailed, trending on artstation.”]
- Column 5:** [“the moon as a lightbulb being unscrewed by someones hand”]

F. More Visual Results

F.1. More Visual Comparisons on FLUX.1

Figure 9 presents additional visual comparisons on FLUX.1. While reuse-based methods exhibit visible degradation in fine details and prediction-based methods show subtle artifacts, PrediT preserves sharp details and accurate color reproduction across diverse prompts, validating the effectiveness of our approach.

F.2. More Visual Comparisons on HunyuanVideo

Figure 10 provides additional visual comparisons on HunyuanVideo. Video generation is more challenging as errors can accumulate across both denoising steps and video frames. Existing methods show blurriness or temporal inconsistencies, while PrediT maintains sharp spatial details and smooth temporal transitions, achieving up to $3.28\times$ speedup while preserving visual quality.

G. Memory Usage Analysis

Video generation with DiT models requires substantial GPU memory due to the large spatial-temporal feature maps. We therefore analyze the memory consumption of different acceleration methods on HunyuanVideo across various resolutions and frame settings using a single NVIDIA A800 80GB GPU. As shown in Table 7, PrediT introduces minimal memory overhead compared to the original model, with only 1%-2% additional memory usage across all settings. In contrast, prediction-based methods require storing Taylor expansion coefficients and historical gradients, leading to out-of-memory (OOM) errors at most settings. PAB also suffers from OOM at higher resolutions due to its attention caching mechanism. TeaCache shows moderate memory increase but remains functional. These results demonstrate that PrediT achieves significant speedup while maintaining memory efficiency, making it practical for real-world video generation applications.

H. Supplementary Results for Ablation Studies

We conduct more ablation studies on DiT-XL/2 to analyze the impact of different hyperparameter configurations. Table 8 shows results with varying predictor order, dynamics threshold, and correction ratio. Higher-order predictors achieve better quality at the cost of reduced speedup, while smaller τ values lead to more frequent corrections and improved quality. Notably, with $\mathcal{O} = 4$ and $\tau = 0.75$, PrediT achieves FID of 2.17, surpassing the baseline, demonstrating that our method can improve quality while accelerating inference.

Table 8. Ablation Study with Different Configurations on ImageNet with DiT-XL/2.

Settings	Latency(s) ↓	Speedup ↑	FID↓	sFID↓	IS↑
DDIM-50	0.569	1.00×	2.28	4.25	242.3
($\mathcal{O} = 2, \tau = 1.25, r = 0.3$)	0.219	2.60×	2.97	5.33	222.6
($\mathcal{O} = 2, \tau = 1.25, r = 0.1$)	0.250	2.28×	3.01	5.24	222.5
($\mathcal{O} = 2, \tau = 1.00, r = 0.3$)	0.251	2.27×	2.71	5.31	228.4
($\mathcal{O} = 2, \tau = 1.00, r = 0.2$)	0.297	1.92×	2.72	5.28	228.3
($\mathcal{O} = 2, \tau = 1.00, r = 0.1$)	0.293	1.94×	2.78	5.30	227.7
($\mathcal{O} = 2, \tau = 0.75, r = 0.3$)	0.291	1.96×	2.44	4.84	235.0
($\mathcal{O} = 2, \tau = 0.75, r = 0.1$)	0.306	1.86×	2.48	4.88	234.3
($\mathcal{O} = 3, \tau = 1.25, r = 0.3$)	0.228	2.50×	2.54	5.12	231.1
($\mathcal{O} = 3, \tau = 1.25, r = 0.1$)	0.259	2.20×	2.49	4.85	232.4
($\mathcal{O} = 3, \tau = 1.00, r = 0.3$)	0.254	2.24×	2.39	4.89	235.8
($\mathcal{O} = 3, \tau = 1.00, r = 0.2$)	0.286	1.99×	2.39	4.89	235.8
($\mathcal{O} = 3, \tau = 1.00, r = 0.1$)	0.287	1.98×	2.37	4.77	237.8
($\mathcal{O} = 3, \tau = 0.75, r = 0.3$)	0.295	1.93×	2.25	4.70	239.7
($\mathcal{O} = 3, \tau = 0.75, r = 0.1$)	0.312	1.82×	2.25	4.65	239.9
($\mathcal{O} = 4, \tau = 1.25, r = 0.3$)	0.240	2.37×	2.41	5.12	234.7
($\mathcal{O} = 4, \tau = 1.25, r = 0.1$)	0.269	2.12×	2.33	4.82	236.8
($\mathcal{O} = 4, \tau = 1.00, r = 0.3$)	0.268	2.12×	2.24	4.78	239.5
($\mathcal{O} = 4, \tau = 1.00, r = 0.2$)	0.302	1.88×	2.24	4.75	239.8
($\mathcal{O} = 4, \tau = 1.00, r = 0.1$)	0.309	1.84×	2.23	4.60	240.1
($\mathcal{O} = 4, \tau = 0.75, r = 0.3$)	0.305	1.87×	2.17	4.61	242.7
($\mathcal{O} = 4, \tau = 0.75, r = 0.1$)	0.324	1.76×	2.16	4.49	243.3

Statement on Large Language Model Usage

In the preparation of this manuscript, Large Language Models (LLMs) were mainly utilized for the purpose of language polishing. The LLM played no role in the generation of core ideas. All final content was thoroughly reviewed and approved by the authors.



Figure 9. More Visual Comparisons on FLUX.1. Zoom in for best viewing.

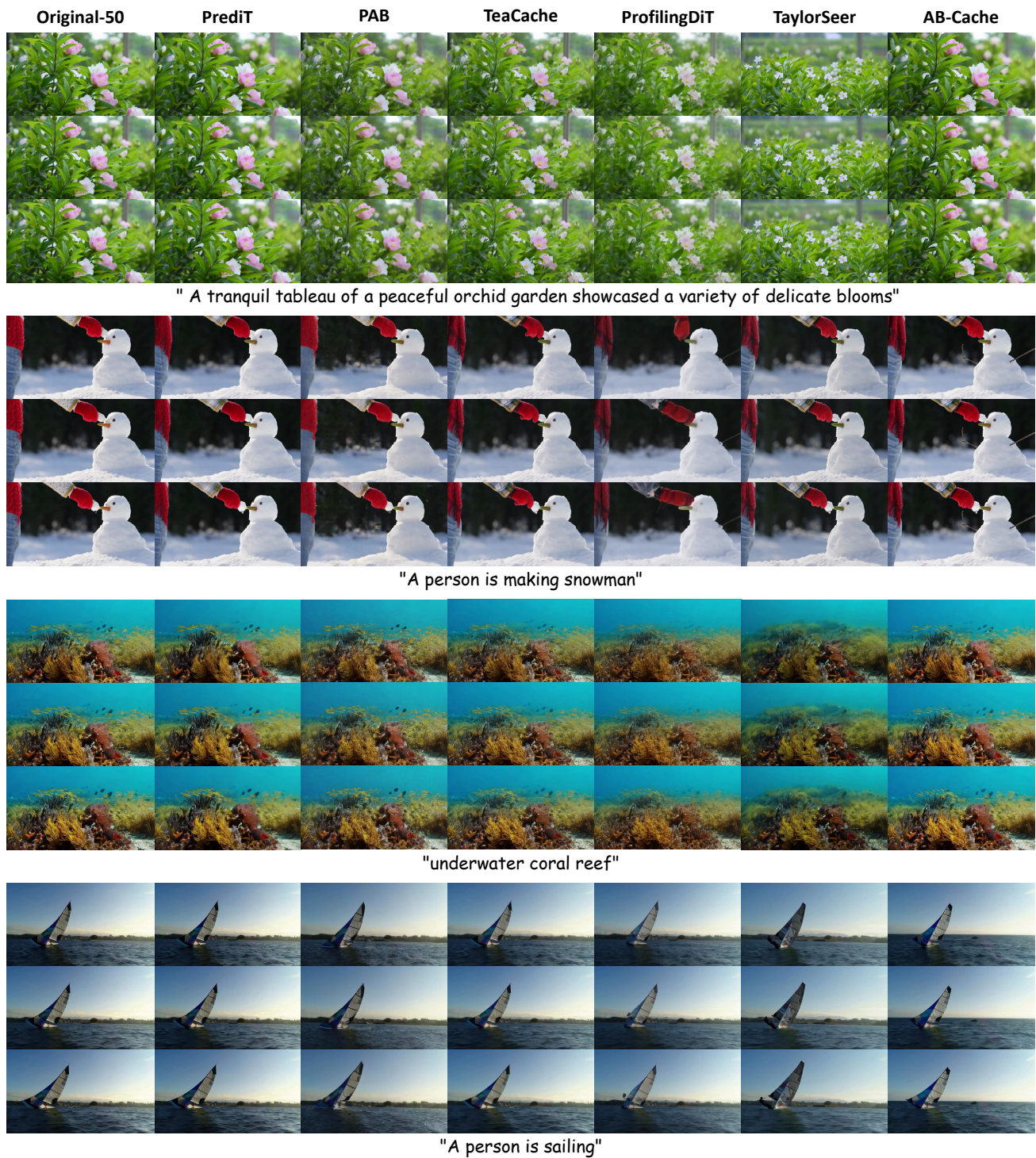


Figure 10. More Visual Comparisons on HunyuanVideo. Zoom in for best viewing.